

XENON10/100 dark matter constraints in comparison with CoGeNT and DAMA: examining the \mathcal{L}_{eff} dependence

Christopher Savage,^{1,*} Graciela Gelmini,^{2,†} Paolo Gondolo,^{3,‡} and Katherine Freese^{4,§}

¹ *The Oskar Klein Centre for Cosmoparticle Physics,
Department of Physics, Stockholm University,
AlbaNova, SE-10691 Stockholm, Sweden*

² *Department of Physics and Astronomy, UCLA,
430 Portola Plaza, Los Angeles, CA 90095, USA*

³ *Department of Physics, University of Utah,
115 S 1400 E #201 Salt Lake City, UT 84112, USA[¶]*

⁴ *Michigan Center for Theoretical Physics, Department of Physics,
University of Michigan, Ann Arbor, MI 48109, USA*

(Dated: July 30, 2010)

Abstract

We consider the compatibility of DAMA/LIBRA, CoGeNT, XENON10 and XENON100 results for spin-independent (SI) dark matter Weakly Interacting Massive Particles (WIMPs), particularly at low masses (~ 10 GeV), assuming a standard dark matter halo. The XENON bounds depend on the scintillation efficiency factor \mathcal{L}_{eff} for which there is considerable uncertainty. Thus we consider various extrapolations for \mathcal{L}_{eff} at low energy. With the \mathcal{L}_{eff} measurements we consider, XENON100 results are found to be insensitive to the low energy extrapolation. We find the strongest bounds are from XENON10, rather than XENON100, due to the lower energy threshold. For reasonable choices of \mathcal{L}_{eff} and for the case of SI elastic scattering, XENON10 is incompatible with the DAMA/LIBRA 3σ region and severely constrains the 7-12 GeV WIMP mass region of interest published by the CoGeNT collaboration.

I. INTRODUCTION

The nature of the dark matter that comprises a quarter of the Universe is one of the big unanswered questions in astrophysics and particle physics. Perhaps the best motivated candidates are Weakly Interacting Massive Particles (WIMPs) which have weakly interacting cross sections and masses in the GeV–10 TeV range. In recent months, there have been new data releases from many experiments that have engendered a great deal of excitement. Of

*savage@fysik.su.se

†gelmini@physics.ucla.edu

‡paolo@physics.utah.edu

§ktfreese@umich.edu

[¶]Also at Korea Institute for Advanced Study, Seoul 130-722, Korea

particular interest is a low mass region ~ 10 GeV which at first sight seems to be compatible with a number of different experiments. The goal of this paper is to examine some of the issues regarding the question of such compatibility. In this paper, we will restrict ourselves here to considering WIMPs with spin-independent (SI) interactions. Spin-dependent and mixed couplings will be examined in a future work.

It was initially the DAMA/NAI experiment [1], looking for annual modulation [2, 3] of a WIMP signal, that found such a possible low mass region. WIMPs with SI interactions in the mass range 5–9 GeV were found to be compatible with the DAMA/NaI results and all negative results from other searches that existed at the time [4, 5]. The situation changed after the publication of the first DAMA/LIBRA results [6] (see *e.g.* Ref. [7] and reference therein). For SI interactions, Ref. [7] found that the best fit DAMA regions were ruled out to the 3σ C.L. But Ref. [7] also found that for WIMP masses of ~ 8 GeV, some parameters outside these regions still yielded a moderately reasonable fit to the DAMA data and were compatible with all 90% C.L. upper limits from negative searches, when ion channeling in the DAMA experiment as understood at the time was included (see Section II B below). The strongest bounds at the time came from CDMS [8] and XENON10 [9]. Since then many new data sets have been released and a reexamination of the light WIMP region is now necessary. We will focus on the following three factors: a possible dark matter signal for 7-12 GeV WIMP's found by the CoGeNT collaboration [10]; the existence of new better upper limits, in particular the bounds set by the XENON10 [11] and XENON100 [12] collaborations; and the recognition that the effect of channeling in NaI(Tl) crystal is less important than previously assumed [13] (see Section II B).

CDMS [14] has released its full data set, with tighter bounds and two unexplained events at low energy that may be compatible with background. CDMS constraints will be included but are not a focus of this paper. Our focus is on elastic scattering of spin-independent WIMPs from a standard Maxwellian halo; recent examinations comparing experimental studies in this case include [15–22].

Just prior to our paper being submitted, a revised version of Ref. [23] appeared that added an examination of XENON100 and \mathcal{L}_{eff} in the context of scalar WIMPs. The halo model parameters and \mathcal{L}_{eff} models used in that paper differ somewhat from ours, but the results are qualitatively similar.

The interpretation of the XENON10 and XENON100 results requires the ability to reliably reconstruct the nuclear recoil energy from the observed signal. This depends on the scintillation efficiency factor \mathcal{L}_{eff} for which there is considerable uncertainty at low energies (see Section II A). A large part of this paper is devoted to examining the \mathcal{L}_{eff} dependence of the two XENON constraints.

In this paper we focus on comparing the following experimental results: the combined modulation signal [1] as well as the total rate [6] from DAMA/NaI and DAMA/LIBRA; the combined CDMS 5-tower results [8, 14]; the recent first results from XENON100 [12]; and the older but lower threshold XENON10 reanalysis results [11]. Constraints for CDMS, XENON10, and XENON100 are determined using the Maximum Gap method¹ [24], while

¹ For zero observed events (as in the case of XENON100), the Maximum Gap (MG) method provides an identical constraint as that produced by a Poisson limit based on the total number of events. When events are observed, the MG method provides better constraints than the Poisson case as the former takes the energy spectrum into account, whereas the latter does not. The use of MG is of particular importance for XENON10 as the 13 observed events have energies that are inconsistent with the spectrum expected for

the parameters compatible with DAMA are determined via the goodness-of-fit of their observed modulation signal with the theoretically expected signal. Details of these statistical analyses may be found in Ref. [7].

For the two XENON experiments, we assume the energy resolution is primarily limited by a Poisson distribution in the small number of photoelectrons (PE) expected at low recoil energies. Interactions in the liquid Xenon comprising the XENON10 and XENON100 detectors give rise to a prompt scintillation signal ($S1$) followed by a delayed secondary scintillation signal ($S2$). The quantities $S1$ and $S2$ are discussed in the following section and the various thresholds and data cuts are described in *e.g.* Ref. [11]. The efficiencies for XENON10 and XENON100 are taken from Refs. [11] and [12], respectively. However, for XENON10, the $S1$ peak finding efficiency factor η_{S1} , which was not included in Ref. [11] (where it was not particularly relevant), must also be taken into account. For this η_{S1} factor, we take the more conservative of the two cases found in Ref. [25].

A second issue must also be taken into account. As explained in detail below, as the recoil energy decreases, so do the average $S1$ and $S2$ signals. At low enough energies, a sizable fraction of the events may fail to produce enough $S2$ signal and/or to fall in the proper $\log(S2/S1)$ range (the nuclear recoil band cut), even if a fluctuation gives a high enough $S1$. At higher recoil energies, the relative size of the fluctuations get smaller and the average $S2$ is too high for any significant fraction of the $S2$ fluctuations to fall below the $S2$ threshold. However, somewhere below an $S1$ average of 1 photoelectron (PE) in XENON10, an event would need not only an upward fluctuation in $S1$, but an upward fluctuation in $S2$ to pass both thresholds and it would require particular ranges of fluctuations to fall within the required range for $\log(S2/S1)$. Thus, to avoid issues with the $S2$ threshold and nuclear recoil band cuts, we ignore recoil energies that give on average less than 1 PE in the $S1$ signal. We find that, with Poisson fluctuations included, low energy recoils in XENON10 tend to pass the various thresholds and cuts at a higher rate than predicted by the efficiencies we use; these efficiencies can thus be considered conservative over the range at which they are applied. Additional events passing these various cuts can arise from low energy recoils that give an average $S1$ signal $\langle S1 \rangle$ that falls below our imposed cutoff of $\langle S1 \rangle \geq 1.0$ PE. Accounting for these events will strengthen the XENON10 constraints at low WIMP masses. Our $\langle S1 \rangle$ cutoff is simply due to the efficiency being unknown for these low energy recoils at this time. We are examining these low energy recoil efficiencies for a future work, though a comprehensive treatment of these efficiencies in XENON10 and XENON100 has appeared in the meantime [26].

In addition to constraints for the above experiments, we also show the 7-12 GeV WIMP mass region suggested by CoGeNT as an explanation for excess events seen at low energies in their detector [10]. We perform our own statistical analyses of all data sets except CoGeNT, for which we simply use their published region.

To allow for direct comparison, all the other experimental constraints are determined using the same 600 km/s galactic halo escape velocity as used by CoGeNT in their analysis [27]. This escape velocity falls within the 90% confidence interval of 498 km/s to 608 km/s that was determined by a recent analysis of high velocity stars [28], but is somewhat above the median likelihood of 544 km/s that was found in that analysis. Similarly, we use throughout the value 220 km/sec (used by CoGeNT) for the rotation velocity of the Galactic disk in the vicinity of the Sun. We note that new measurements suggest that the rotation velocity might

a light elastically scattering WIMP.

be higher, 254 ± 16 km/s [29], the effect of which is to shift the best fit in all experiments to slightly lower WIMP masses [30].

Comparison with Version One of this paper: We have made two substantial changes, as discussed in the previous paragraphs. First, we have included the effects of η_{S1} , the $S1$ peak finding efficiency factor. With this factor included, the XENON10 constraints shift upwards in scattering cross-section by at most $\sim \times 1.7$ at any given WIMP mass, not by several orders of magnitude (as was speculated in Ref. [31]). Second, in the current version we do not include recoil energies which yield on average less than 1.0 PE in the $S1$ signal. It is this second issue that is by far the bigger effect. A more complete discussion can be found in the Appendix. In addition, in the Appendix we respond to various critiques of our work.

II. EXPERIMENTAL ISSUES: \mathcal{L}_{eff} AND CHANNELING

In this section we discuss two important experimental issues. First, the scintillation factor in XENON \mathcal{L}_{eff} is extremely important in interpreting results and yet is not well known. Second, the channeling effect in DAMA/LIBRA, again not well known, may change the location of the regions in WIMP parameter space that are compatible with the data.

A. The \mathcal{L}_{eff} Scintillation Efficiency Factor in XENON

The interpretation of the XENON10 and XENON100 results requires the ability to reliably reconstruct the nuclear recoil energy from the observed signal. This reconstruction depends on the scintillation efficiency factor \mathcal{L}_{eff} for which there is considerable uncertainty at low energies. Here we discuss this factor and present three models for \mathcal{L}_{eff} at low energy.

Interactions in the liquid Xenon comprising the XENON10 and XENON100 detectors give rise to a prompt scintillation signal, $S1$, followed by a delayed secondary scintillation signal, $S2$. The $S1$ signal arises from a rapid relaxation of excited Xenon states produced as a result of the interaction. The $S2$ signal arises from ionized electrons also produced in the interaction; these drift through the liquid xenon under an applied electric field, but once they reach the liquid surface they are extracted into a xenon gas phase where they emit proportional scintillation light. The drift time of the electrons causes this secondary scintillation (the $S2$ signal) to be observed later than the $S1$ signal, allowing both scintillation signals to be measured separately. The $S1$ signal can be used to determine the energy of the interaction, while the combination of both signals allows discrimination between nuclear recoil events (possibly WIMP interactions) and electron recoil events (necessarily background interactions). The ratio of $S2$ to $S1$ is much higher in the case of electron recoils than in the case of nuclear recoils.

Interpretation of the XENON results requires the ability to reliably reconstruct the nuclear recoil energy E_{nr} from the observed $S1$ signal. Calibration of the nuclear recoil energy dependence of $S1$ often involves gauging the detector's response to electron recoils at higher energies; parts of the detector's response (*e.g.* the fraction of scintillation photons that yield photoelectrons (PE) in the photodetectors) are more easily determined in this case than with nuclear recoils at lower energies. Taking $S1$ to be normalized to the number of PE, $S1$ and E_{nr} are related by an equation involving the higher energy electron recoil calibrations:

$$S1 = (S_{nr}/S_{ee}) \mathcal{L}_{\text{eff}}(E_{nr}) L_y E_{nr} . \quad (1)$$

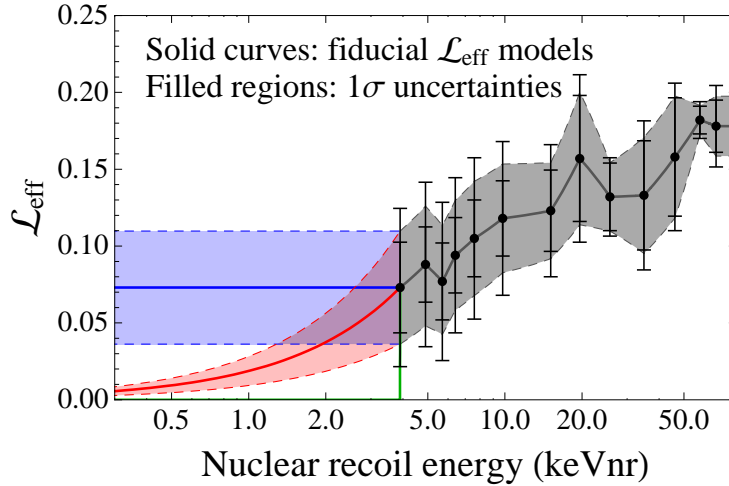


FIG. 1: \mathcal{L}_{eff} as a function of recoil energy. The points correspond to the measurements of Manzur *et al.* [42] with statistical and systematic errors in \mathcal{L}_{eff} as indicated (uncertainties in recoil energy not shown). Solid curves show the fiducial \mathcal{L}_{eff} dependence used in this work. Filled regions/dashed curves indicate the 1σ variation in the \mathcal{L}_{eff} dependence. At 3.9 keVnr (the lowest energy data point), $\mathcal{L}_{\text{eff}} = 0.073^{+0.034+0.018}_{-0.025-0.026} \approx 0.073 \pm 0.037$. At lower energies three cases are examined: constant \mathcal{L}_{eff} (blue) at the above value, \mathcal{L}_{eff} falling linearly to zero at zero energy (red), and \mathcal{L}_{eff} equal to zero (green). Above 3.9 keVnr, the gray curve and region are used in all cases. Note linear relationships appear curved in the figure due to the logarithmic scaling.

Here, L_y is the light yield in PE/keVee for 122 keVee γ -rays². $\mathcal{L}_{\text{eff}}(E_{nr})$ is the scintillation efficiency of nuclear recoils relative to 122 keVee γ -rays in zero electric field; this factor is a function of the nuclear recoil energy. Since there is an applied electric field in the experiment, which reduces the scintillation yield by quickly removing charged particles from the original interaction region, two additional factors must be taken into account: S_{ee} and S_{nr} are the suppression in the scintillation yield for electronic and nuclear recoils, respectively, due to the presence of the electric field in the detector volume. The quantities S_{ee} , S_{nr} , and L_y are detector dependent; \mathcal{L}_{eff} is not.

Recent comments have drawn attention to the role that \mathcal{L}_{eff} determinations play in setting experimental constraints for Xenon-based detectors [32–34]. A variety of \mathcal{L}_{eff} measurements have been made over the years [35–42], but limited statistics and systematics issues have so far prevented a clear picture from emerging as to the behavior of \mathcal{L}_{eff} at low recoil energies. There are two primary issues in debate: (1) Which of the \mathcal{L}_{eff} measurements should be used as a basis for analyzing direct detection results? and (2) Measurements of \mathcal{L}_{eff} have only been made at energies above some minimum; what is the behavior of \mathcal{L}_{eff} at low energies, where no measurements have as yet been made? For the first issue, the XENON100 collaboration has chosen to use a global fit to multiple \mathcal{L}_{eff} measurements in their analysis, whereas Ref. [32] suggests that the recent measurements by Manzur *et al.* [42] should be used; in both cases, \mathcal{L}_{eff} measurements are based upon fixed energy neutron scatters. We do not contribute

² The unit “keVee” refers to the electron-equivalent energy in keV, the amount of energy in an electron recoil event that would produce a given scintillation signal in the detector (whether or not the scintillation was, in fact, produced by an electron recoil). The unit “keVnr” refers to the nuclear recoil energy in keV.

to the debate as to which \mathcal{L}_{eff} data sets are most appropriate; however, in the interest of examining the most conservative XENON constraints, we use the Manzur *et al.* data alone in our analyses.

The choice of \mathcal{L}_{eff} measurements to use in the XENON analyses has a significant impact on the resulting constraints for low WIMP masses. The Manzur *et al.* data yield the lowest values for \mathcal{L}_{eff} among the fixed-energy neutron scatter measurements, implying the highest recoil energy thresholds and therefore the lowest sensitivity for the XENON detectors to low mass WIMPs (which generate only low energy recoils). The Manzur *et al.* data is shown in Figure 1.

A comment is in order about the lower ZEPLIN-III \mathcal{L}_{eff} measurement [43] represented as a band in Fig. 1 of [32]. ZEPLIN fits a nonlinear \mathcal{L}_{eff} model to their broad spectrum nuclear recoil calibration data to obtain \mathcal{L}_{eff} curves that were used in their analysis. These fits suggest a constant \mathcal{L}_{eff} at recoil energies above ~ 30 keVnr, with \mathcal{L}_{eff} sharply falling at energies below ~ 20 keVnr and approaching zero at ~ 7 -8 keVnr; see Figure 15 of Ref. [43] and the accompanying text. Thus the suggestion has been made by nonmembers of the ZEPLIN team [31] that \mathcal{L}_{eff} should be taken to be zero below ~ 8 keVnr as a conservative model of \mathcal{L}_{eff} . This \mathcal{L}_{eff} model would yield significantly weaker XENON constraints relative to what we have referred to as conservative models based on the Manzur *et al.* measurements of \mathcal{L}_{eff} [42]. However, the members of the ZEPLIN experiment themselves do not advocate their fits as being an indicator of \mathcal{L}_{eff} behavior at recoil energies below ~ 8 keVnr [44]. In addition, the dependence of these curves on statistical and systematic uncertainties has not been fully determined, where these uncertainties can significantly impact the lowest recoil energy portion of their fits. The ZEPLIN-III dark matter analysis is, in fact, mainly insensitive to the low recoil energy portion of their \mathcal{L}_{eff} curves. Further discussion of the ZEPLIN data can be found in the Appendix. Moreover, as explained in detail in the Appendix, below the recoil energies of 7 keVnr, the Manzur *et al.* measurements are incompatible with $\mathcal{L}_{\text{eff}} = 0$ at far more than the 3σ level. We consider the Manzur *et al.* measurements more reliable than the ZEPLIN-III estimate of \mathcal{L}_{eff} at low energies.

The second issue in debate is how \mathcal{L}_{eff} behaves at energies below where measurements have been made. Most \mathcal{L}_{eff} measurements are at recoil energies above 5 keVnr; Manzur *et al.* have a measurement at 3.9 ± 0.9 keVnr. The \mathcal{L}_{eff} behavior below these energies is unclear from an experimental and theoretical standpoint, at least at the precision necessary for use in a WIMP constraint analysis. The XENON collaboration has suggested that \mathcal{L}_{eff} measurements are consistent with \mathcal{L}_{eff} being effectively constant at low recoil energies, at least at energies where recoils may contribute to their signal [12, 40, 41]. Various \mathcal{L}_{eff} measurements are also consistent with an \mathcal{L}_{eff} that decreases as one goes to lower recoil energies; see *e.g.* Sect. V of Ref. [42] which provides a theoretically motivated empirical model of such a decreasing \mathcal{L}_{eff} . Furthermore, Ref. [32] states that “the mechanisms behind the generation of *any* significant amount of scintillation are still unknown and may simply be absent at the few keVnr level.” Given this uncertainty we use three different extrapolations of \mathcal{L}_{eff} at low energies: constant, decreasing as one goes to lower recoil energies, or just zero.

We choose as our fiducial \mathcal{L}_{eff} model a piecewise linear interpolation between the central Manzur *et al.* values at their measured energies, shown in Figure 1. In addition, we will also examine similarly constructed \mathcal{L}_{eff} models using the 1σ uncertainties in the Manzur *et al.* measurements³. The choice of linear interpolation vs. a quadratic interpolation or spline

³ The statistical and systematic errors in the measured \mathcal{L}_{eff} are added in quadrature with the upper and

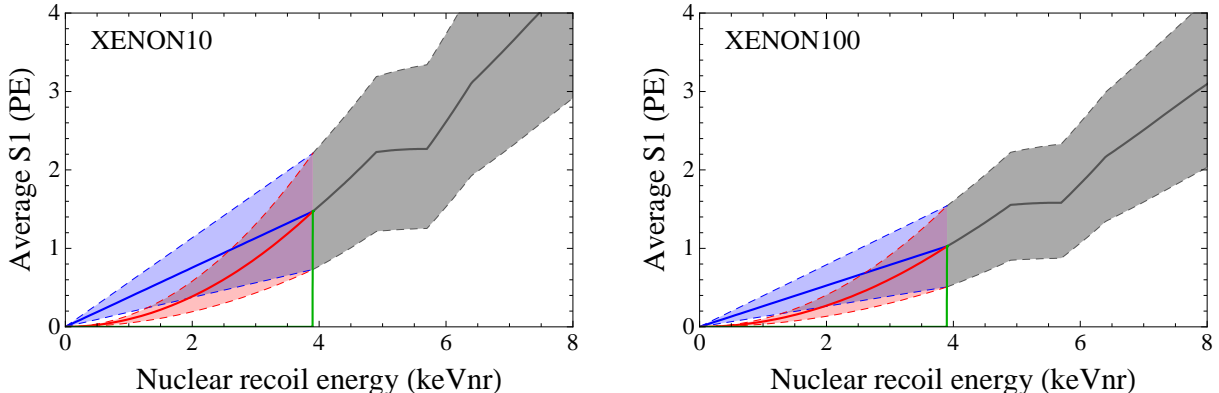


FIG. 2: The average $S1$ signal as a function of nuclear recoil energy for XENON10 (left) and XENON100 (right). Curves and regions correspond to the \mathcal{L}_{eff} models shown in Figure 1.

fit to the \mathcal{L}_{eff} points has a negligible impact on the generated constraints compared to that from the 1σ variations in the \mathcal{L}_{eff} points themselves. Below recoil energies of 3.9 keVnr, the lowest Manzur *et al.* measurement⁴, we examine three behaviors for \mathcal{L}_{eff} , also shown in Figure 1: (1) a constant \mathcal{L}_{eff} , (2) an \mathcal{L}_{eff} that goes linearly to zero at zero recoil energy, and (3) an \mathcal{L}_{eff} that is strictly zero. Even if the scintillation goes to zero at some low but finite recoil energy, there is no reason to expect this to occur above $\sim 2\text{--}3$ keVnr; the measurements of \mathcal{L}_{eff} provide no indication of an abrupt (rather than gradual) falling of \mathcal{L}_{eff} at energies just below where the measurements exist. As such, the third case is perhaps unrealistically conservative, but never-the-less provides the most conservative case. In addition, the use of this case will allow us to examine the contribution of low energy recoils in generating constraints. The average $S1$ signals as a function of the nuclear recoil energy E_{nr} that correspond to these \mathcal{L}_{eff} models are shown in Figure 2 for XENON10 and XENON100.

In the interest of examining the most conservative XENON constraints, we base all three cases on the data from Manzur *et al.* [42]. Of the existing data sets, the Manzur *et al.* data yield the lowest values for \mathcal{L}_{eff} , implying higher recoil energy thresholds for the XENON experiments, and thereby reducing the sensitivity of XENON to low mass WIMPs.

B. Channeling Effects in DAMA/LIBRA

The channeling effect is of crucial importance when considering the compatibility of DAMA with other experimental results as this effect has the potential to significantly alter the WIMP masses and cross-sections which are compatible with the DAMA modulation signal.

lower uncertainties averaged; uncertainties in the corresponding recoil energies for those measurements have been neglected.

⁴ Manzur *et al.* measure $\mathcal{L}_{\text{eff}} = 0.073_{-0.025-0.026}^{+0.034+0.018} \approx 0.073 \pm 0.037$ at 3.9 keVnr, where the two errors in the first case are the statistical and systematic uncertainties, respectively, and the second case is the combined uncertainty as described in the previous footnote.

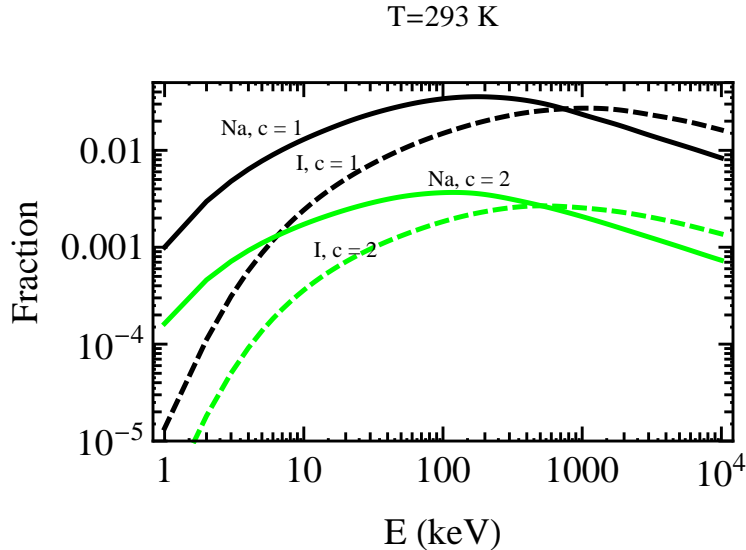


FIG. 3: Upper bounds to the channeling fraction at a temperature of 293 K for Na (solid lines) and I (dashed lines) recoiling ions in a NaI crystal for two different models of the temperature effect in the lattice parameterized with $c = 1$ (black) and $c = 2$ (green or gray). No dechanneling processes are taken here into account. To be conservative, in this paper we will use the $c = 1$ results presented here, as they yield the largest change in the DAMA compatible regions of parameter space relative to the no-channeling case. This figure is reproduced from Ref. [13], where further details may be found.

Channeling and blocking effects in crystals refer to the orientation dependence of charged ion penetration in crystals. In the “channeling effect,” ions incident upon a crystal along symmetry axes and planes suffer a series of small-angle scattering that maintain them in the open “channels” in between the rows or planes of lattice atoms and thus penetrate much further into the crystal than in other directions. Channeled incident ions do not get close to lattice sites, where they would be deflected at large angles, and they lose energy almost exclusively into electrons. The “blocking effect” consists in a reduction of the flux of ions originating in lattice sites along symmetry axes and planes, creating what is called a “blocking dip” in the flux of ions exiting from a thin enough crystal as a function of the exit angle with respect to a particular symmetry axis or plane. The potential importance of the channeling effect for direct dark matter detection was first pointed out by H. Sekiya *et al.* [45] and subsequently for NaI(Tl) by Drobyshovski [46] and by the DAMA collaboration [47]. When Na or I ions recoiling after a collision with a dark matter WIMP are channeled, their quenching factor⁵ is approximately $Q = 1$ instead of $Q_I = 0.09$ and $Q_{Na} = 0.3$, since they give their energy to electrons. The DAMA collaboration [47] estimated the fraction of channeled recoils and found it to be large for low recoiling energies in the keV range. Using this evaluation of the channeling fraction, the regions in cross-section versus mass of acceptable

⁵ The quenching factor Q is the ratio of ionization or scintillation produced by a nuclear recoil event in a crystal relative to that produced in an electron recoil event of the same energy. This is analogous to the \mathcal{L}_{eff} factor in liquid Xenon and is likewise used to reconstruct the nuclear recoil energy from the observed ionization/scintillation of an event.

WIMP models in agreement with the DAMA data were found to be considerably shifted towards lower WIMP masses and cross-sections.

However, the DAMA calculation of the channeling fraction did not take into account that the recoiling lattice ions start initially from lattice sites (or very close to them) and, therefore, blocking effects are important. In fact, as argued originally by Lindhard [48], in a perfect lattice and in the absence of energy-loss processes, the probability of a particle starting from a lattice site to be channeled would be zero. The argument uses statistical mechanics in which the probability of particle paths related by time-reversal is the same. In a perfectly rigid lattice, the fraction of channeled recoils would, in fact, be zero. However, the atoms in a crystal are actually vibrating about their equilibrium positions in the lattice. It is this displacement from equilibrium that allows for a non-zero channeling probability of recoiling ions. The vibration amplitude increases with the temperature, thus the effect is temperature dependent: in general the channeling fraction increases with temperature.

Upper bounds to the recoiling channeling fractions in NaI(Tl) crystals at 20°C were obtained in Ref. [13], using analytic models of channeling developed since the 1960's, when channeling was discovered (see for example Refs. [48–50] and references therein). These upper bounds on the channeling fractions were obtained with temperature effects taken into account not only through the vibrations of the colliding nucleus but also in the lattice. The latter depend on the parameter c (see Ref. [13] for details) which in the relevant literature is found to be a number between 1 and 2, with 1 giving the largest channeling fractions (see Figure 3, reproduced from Ref. [13]).

The fractions shown in Figure 3 are also an upper bound in that no dechanneling mechanism has been taken into account to compute them. The collisions with Tl impurities would take channeled ions out of their channel, and this process is not included (see Ref. [13] for further explanations).

III. RESULTS AND DISCUSSION

In Figure 4, we show the WIMP masses and SI cross-sections compatible with the DAMA modulation signal both with and without channeling included; contours are shown for regions compatible at the 7σ , 5σ , 3σ , and 90% level (in order from larger to smaller regions). For the channeling, we use the largest channeling fractions shown in Figure 3 as they provide the largest potential effect on the DAMA constraints. Figure 4 shows that even in this case there is negligible difference between the channeling and non-channeling scenarios except for regions incompatible with DAMA at greater than the 5σ level. Even in these cases, the difference lies only at WIMP masses below 4 GeV and at relatively high SI cross-sections. As channeling is a negligible effect, we do not further include it.

Compared to our previous analysis in [7], the current study takes advantage of additional recently released DAMA data. The effect of the additional data has been to sharpen the regions in parameter space that match the data. For example, at 5σ , there are now two completely separate regions (peaked at different WIMP masses) that were previously joined. In our current work we also display a 7σ contour in which the two regions are again connected. We remind the reader that we are using the goodness-of-fit statistic described in detail in Ref. [7].

Our main results are shown in Figs. (5)-(7), corresponding to the three cases for the behavior of \mathcal{L}_{eff} at low recoil energies. The solid gray contours indicate the WIMP parameters compatible with the DAMA modulation within the 5σ , 3σ , and 90% level; the 5σ DAMA

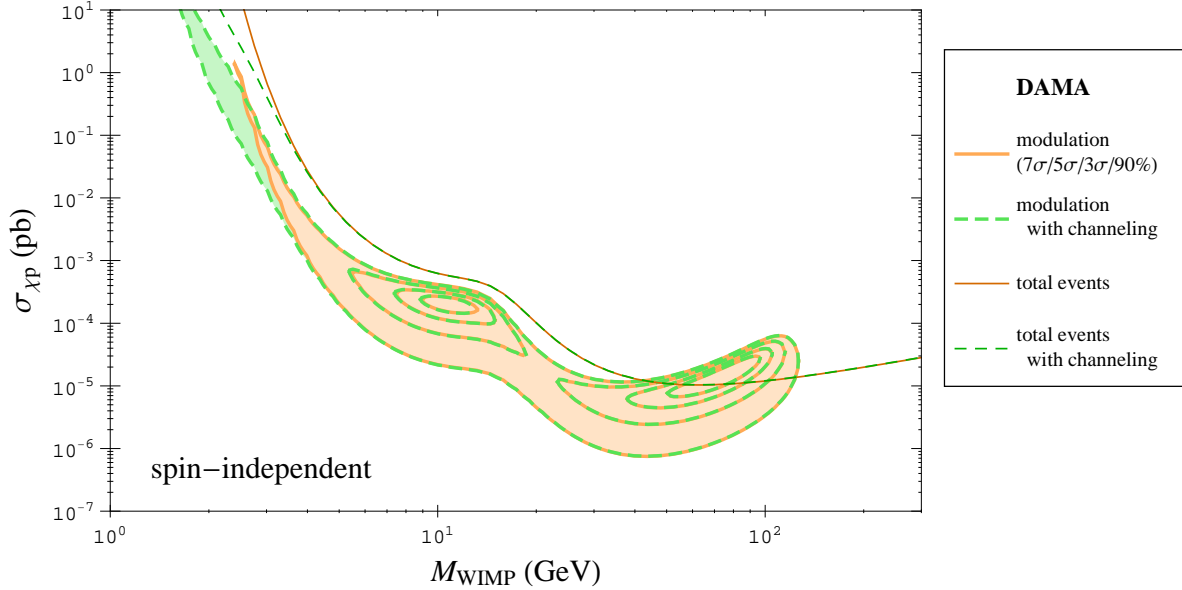


FIG. 4: WIMP masses and spin-independent (SI) cross-sections compatible with the DAMA modulation signal and total number of events, determined with (dashed green) and without (solid orange) the channeling effect included. The largest channeling fractions shown in Figure 3 (taken from Ref. [13]) are used here for the channeling case. Comparing the cases with or without channeling, we find negligible difference in the DAMA modulation regions at the 90%, 3σ , and 5σ levels; only the 7σ contours differ and only for WIMP masses below 4 GeV. The lower and higher mass DAMA regions correspond to parameters where the modulation signals arise from scattering predominantly off of Na and I, respectively.

region is also shaded light gray. The (filled) pink contour corresponds to the 7-12 GeV WIMP mass region suggested by CoGeNT (we reiterate that we have not reanalyzed their data and simply display their published region here). CDMS, DAMA (total events), XENON10, and XENON100 curves indicate regions for which the WIMP parameters are excluded at the 90% level (the parameters above these curves are excluded). The solid green region for XENON10 and solid purple region for XENON100 do *not* indicate regions compatible within a given level (as opposed to the DAMA and CoGeNT regions); they instead indicate how the 90% exclusion constraints vary with the 1σ level uncertainties in the \mathcal{L}_{eff} measurements. Overlapping XENON10 and XENON100 1σ regions are shown in blue.

For the fiducial (central value) \mathcal{L}_{eff} model in the case where it is constant below 3.9 keVnr, shown in Figure 5, the XENON100 constraint excludes all of the DAMA 3σ region, but only the portion of the CoGeNT region with WIMP masses above 9 GeV. We note that, because we use only the Manzur *et al.* \mathcal{L}_{eff} data [42], this constraint is weaker than that presented by XENON100 [12]. If the 1σ uncertainties in \mathcal{L}_{eff} are included, XENON100 could exclude nearly all of the DAMA 5σ region and the entire CoGeNT region, if the largest value of \mathcal{L}_{eff} in the 1σ region is taken. On the other hand, it might exclude only the CoGeNT region above 11 GeV and not even all of the DAMA 90% region, if the lowest value of \mathcal{L}_{eff} in the 1σ region is used. However, the CDMS constraint, unaffected by the issues with \mathcal{L}_{eff} , constrains the same CoGeNT region as the fiducial XENON100 case here, with a slighter weaker constraint on the DAMA region (incompatible with the DAMA 2σ region, not shown).

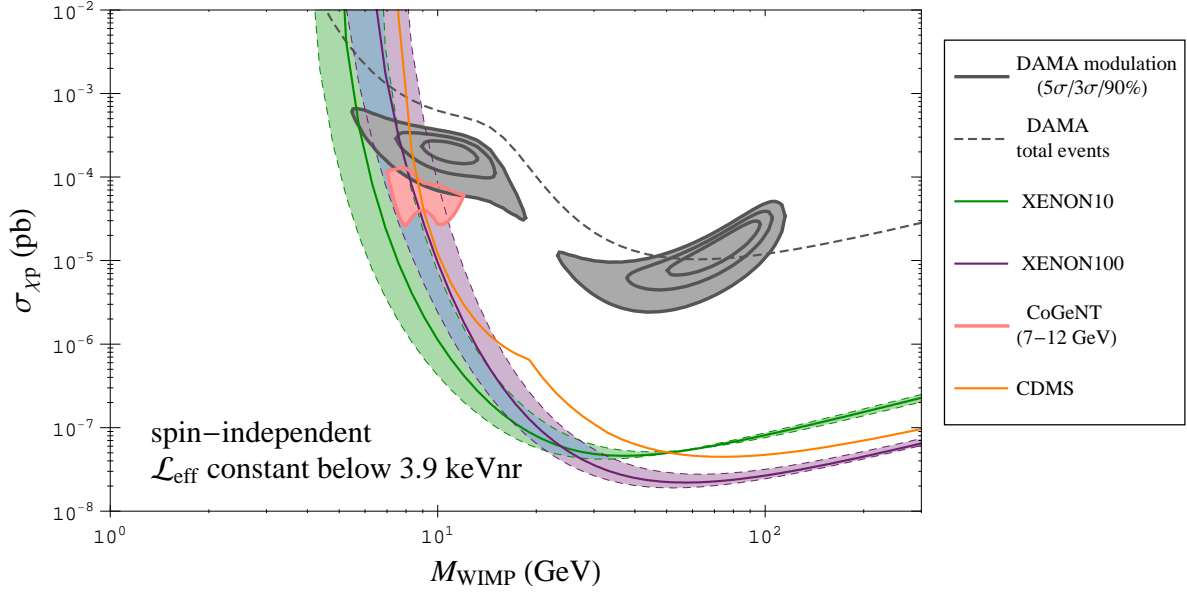


FIG. 5: XENON10 (green) and XENON100 (purple) 90% C.L. constraints for a constant \mathcal{L}_{eff} at recoil energies below 3.9 keVnr. The solid curves are the constraints using the central values of \mathcal{L}_{eff} as described in the text; dashed curves and lighter filled regions indicate how these 90% constraints vary with the 1σ uncertainties in \mathcal{L}_{eff} . The blue region indicates an overlap between the XENON10 (green) and XENON100 (purple) 1σ regions. Also shown are the CDMS constraint (orange curve), DAMA modulation compatible regions (gray contours/region), and the CoGeNT 7-12 GeV region (pink contour/region). The lower and higher mass DAMA regions correspond to parameters where the modulation signals arise from scattering predominantly off of Na and I, respectively.

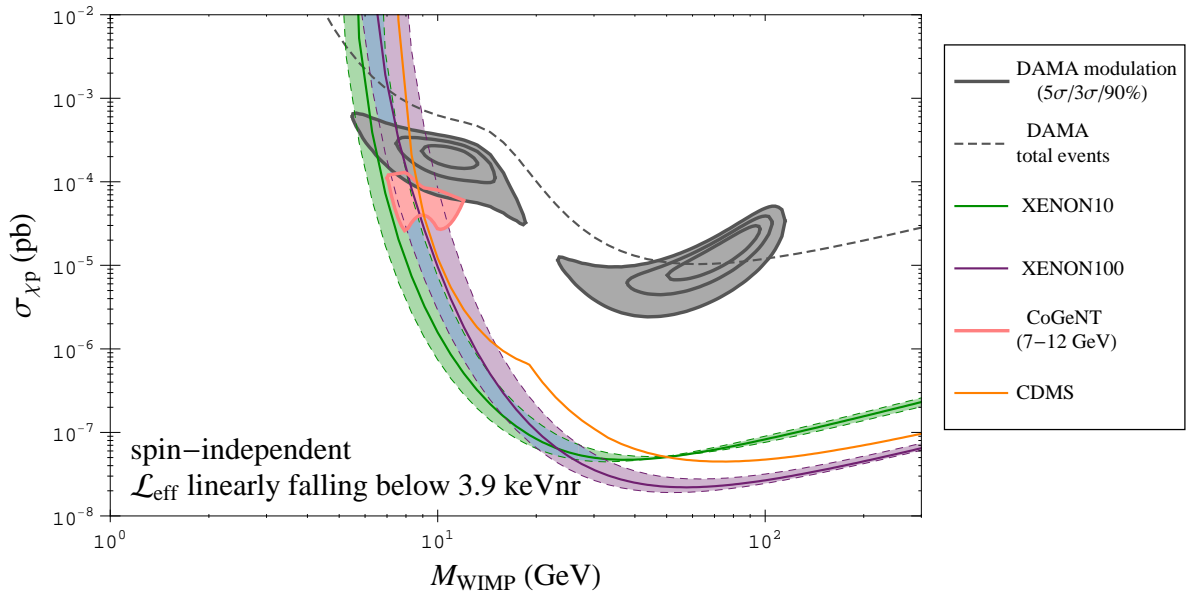


FIG. 6: Same as Figure 5, but taking \mathcal{L}_{eff} to fall linearly to zero for recoil energies below 3.9 keVnr.

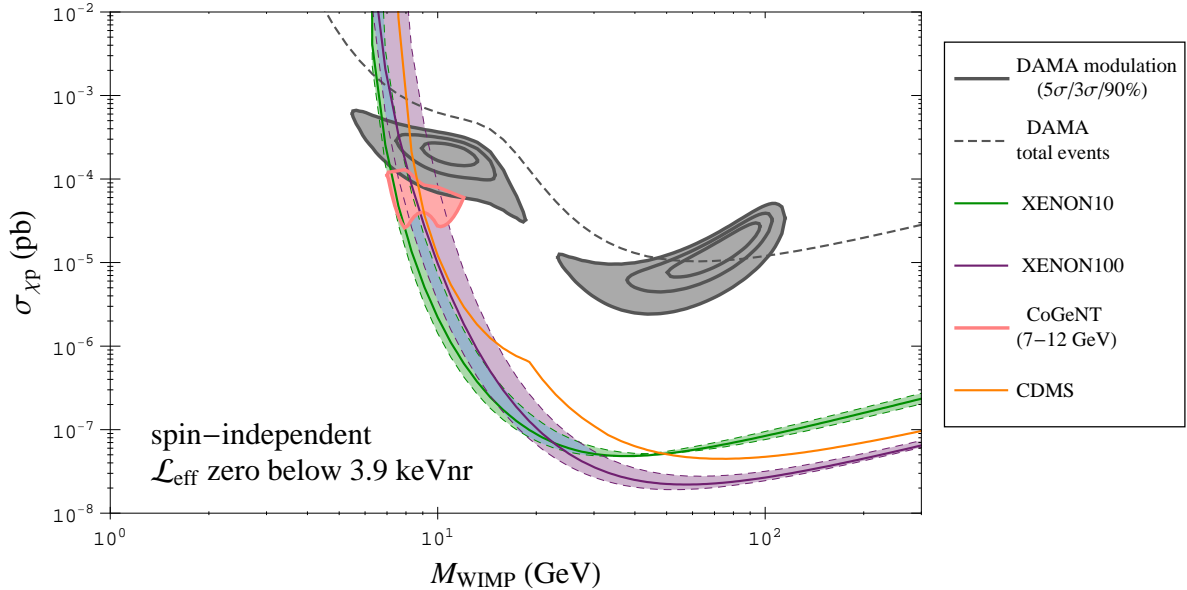


FIG. 7: Same as Figure 5, but taking \mathcal{L}_{eff} to be zero for recoil energies below 3.9 keVnr.

For the fiducial (central value) \mathcal{L}_{eff} model in the case where it falls linearly to zero at zero recoil energy, shown in Figure 6, the XENON100 constraint again excludes nearly all of the DAMA 3σ region and the portion of the CoGeNT region with WIMP masses above 9 GeV. The 1σ variations in the \mathcal{L}_{eff} measurements also yield a similar variation in the XENON100 constraint as they did in the constant \mathcal{L}_{eff} case. The most extreme case, taking \mathcal{L}_{eff} to be zero below 3.9 keVnr, yields similar XENON100 constraints as the other two cases, as seen in Figure 7, although the constraint using the 1σ upper values of \mathcal{L}_{eff} does not quite exclude the full CoGeNT region, leaving a narrow window at WIMP masses of 7-8 GeV. It should be emphasized, however, that the linearly falling \mathcal{L}_{eff} case is already conservative and taking \mathcal{L}_{eff} to be zero below 3.9 keVnr is perhaps unrealistically conservative.

The XENON100 constraints are nearly identical in the DAMA and CoGeNT regions for all three cases of low energy \mathcal{L}_{eff} behavior. In fact, the constraints based on the central and 1σ lower values of \mathcal{L}_{eff} are identical; only when using the upper 1σ \mathcal{L}_{eff} values do the constraints differ. There are two main reasons for the similarity among the constraints: (1) the imposed $\langle S1 \rangle \geq 1.0$ PE cutoff and (2) the small potential contribution from recoil events with energies below 3.9 keVnr where the \mathcal{L}_{eff} models differ. As can be seen in Figure 2, a recoil energy of 3.9 keVnr yields an average $S1$ signal of 1.0 PE in XENON100 when using any of the three fiducial \mathcal{L}_{eff} models. With the $\langle S1 \rangle$ cutoff, there is no contribution from recoils at energies below 3.9 keVnr where the fiducial \mathcal{L}_{eff} models differ; thus, these constraints are identical. When using the 1σ lower values of \mathcal{L}_{eff} , no recoils below 5.9 keVnr are included, so the lesser constraining portion of the 1σ XENON100 constraint bands shown in the figures are likewise identical. On the other hand, when using the 1σ upper values of \mathcal{L}_{eff} , the $\langle S1 \rangle \geq 1.0$ PE cutoff corresponds to recoil energies of 2.5, 3.1, and 3.9 keVnr for the constant, linearly falling, and zero low energy \mathcal{L}_{eff} models, respectively. In this case, low energy recoils contribute to the constraints. However, these low energy recoils can make only a small contribution to the observed signal, as will be discussed below.

As the potential effect of the low energy \mathcal{L}_{eff} behavior on the XENON100 constraints is

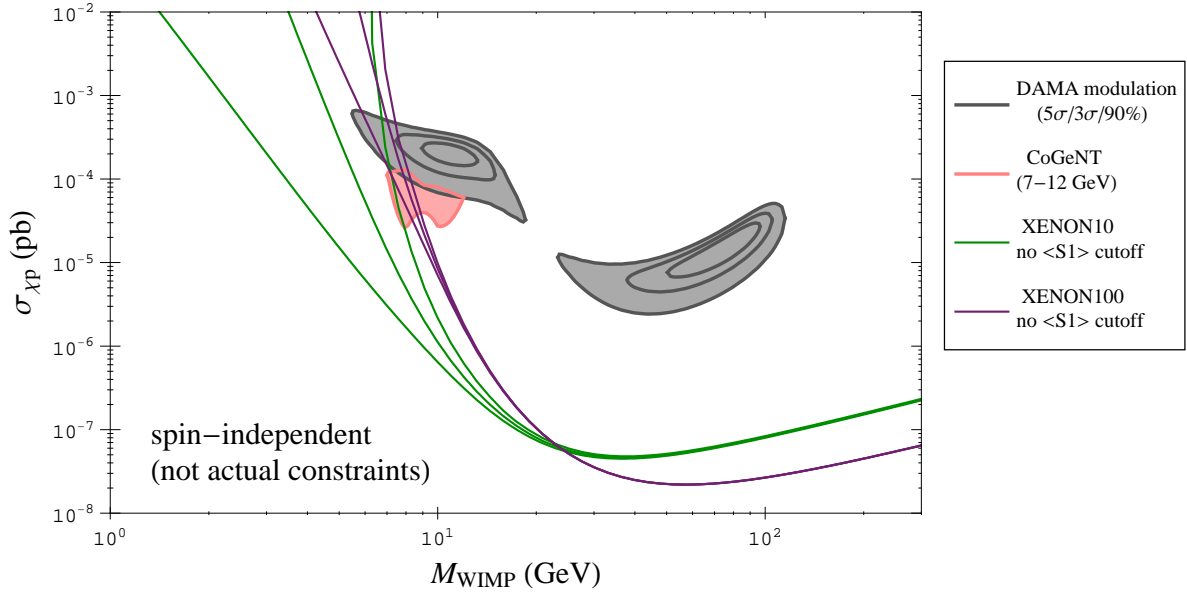


FIG. 8: XENON10 and XENON100 constraints when relaxing the $\langle S1 \rangle \geq 1$ PE cutoff. Only the constraints for the fiducial (central) \mathcal{L}_{eff} models are shown; from left to right, these correspond to constant, linearly falling, and zero \mathcal{L}_{eff} below 3.9 keVnr. To illustrate the potential effect of the low recoil energy behavior of \mathcal{L}_{eff} , these constraints are generated by arbitrarily assuming the nuclear recoil band cut efficiency is constant at low recoil energies. This efficiency should actually fall at sufficiently low recoil energies (for XENON10, at energies that yield an average $S1$ somewhere below 1 PE); these constraints should therefore not be taken as true constraints on the WIMP mass and cross-section. The actual constraints based upon a proper accounting of the efficiencies at low recoil energies will fall somewhere between the constraints shown here and in the previous figures.

masked by the $\langle S1 \rangle \geq 1.0$ PE cutoff, we show in Figure 8 the XENON100 constraints for the three fiducial \mathcal{L}_{eff} models when this cutoff is relaxed. In this figure, we have arbitrarily assumed the nuclear recoil band cut efficiency is constant at low recoil energies. In reality, this efficiency should fall at very low recoil energies and this approximation becomes inappropriate at recoil energies that yield $\langle S1 \rangle$ somewhere below 1 PE. For this reason, these constraints should not be taken to be valid constraints; we show them only to illustrate the potential effect of low energy recoils and the low energy \mathcal{L}_{eff} behavior. With all cut efficiencies properly taken into account, the true constraints would lie somewhere between the constraints shown in this figure and those shown in the previous figures.

With the relaxing of the $\langle S1 \rangle$ cutoff, the XENON100 constraints are still nearly identical in the DAMA and CoGeNT regions for all three cases of low energy \mathcal{L}_{eff} behavior. These constraints are very similar to the ones found in the previous figures, when a $\langle S1 \rangle$ cutoff was included, and are actually identical for the zero \mathcal{L}_{eff} model as this model has no contributions from recoils with $\langle S1 \rangle < 1.0$ PE anyways. The three cases only begin to differ significantly in the low mass, high cross-section parameter space located around and above the DAMA regions in this figure. This can be explained by the XENON100 $S1$ analysis threshold of 4 PE's (the full analysis range is 4-20 PE's). In the absence of a finite energy resolution, this corresponds to a nuclear recoil energy of 9.5 keVnr in our fiducial \mathcal{L}_{eff} models, well

into the energy range where the \mathcal{L}_{eff} behavior is known. With a Poisson fluctuation in the number of observed PE's, recoils at lower energies have a finite chance of producing 4 or more PE's and falling into the analysis range, even if the average number of PE's for events at those energies is below 4. However, at 3.9 keVnr, the average expected number of PE's is 1.0; only 1.9% of such events yield 4 or more PE's. Recoils of 3 keVnr yield an average number of expected PE's of 0.79 and 0.61 for the constant and falling \mathcal{L}_{eff} cases, respectively, with corresponding probabilities of being observed (4+ PE's) of 0.87% and 0.36% (the third case, zero \mathcal{L}_{eff} , produces no PE's at these energies). The small fraction of recoil events with energies below 3.9 keVnr that will be observed in the analysis range means that their contribution is only significant when there are essentially no events at higher energies (due to low WIMP masses and a finite escape velocity in the halo), but to produce a sufficient number of events to fall into the analysis range requires a very large number of WIMP scatters in the $\sim 1\text{-}4$ keVnr range, which requires a high WIMP cross-section. Thus, even when using an overly optimistic nuclear recoil band efficiency, the three \mathcal{L}_{eff} cases can only result in different constraints in the low mass, high cross-section region. This is not necessarily the case for \mathcal{L}_{eff} curves based on measurements that yield values higher than Manzur *et al.*, as this would push the analysis range corresponding to 4-20 PE's to lower recoil energies; such cases, however, inevitably move the XENON100 constraints to the left. In any case, the most significant issue in the XENON100 analysis is the choice of \mathcal{L}_{eff} measurements used to determine the \mathcal{L}_{eff} dependence, not the \mathcal{L}_{eff} behavior at low energies.

We now turn to the XENON10 bounds. We have reanalyzed the XENON10 results in terms of the same \mathcal{L}_{eff} models as used for XENON100 and discussed in the previous section; our results differ from those shown by the XENON collaboration due to the difference in \mathcal{L}_{eff} used in their analyses and ours. The XENON10 results are important because of the lower $S1$ threshold of about 2 PE's used in that analysis, which corresponds to 4.6 keVnr nuclear recoil energies in our fiducial \mathcal{L}_{eff} models (neglecting Poisson fluctuations), much lower than the 9.5 keVnr of the XENON100 4 PE threshold. Because of the lower threshold, the behavior of \mathcal{L}_{eff} at low recoil energies is relevant in producing the XENON10 constraints as Poisson fluctuations allow for a non-trivial probability of seeing 2+ PE's for recoil energies below 3.9 keVnr.

For the constant \mathcal{L}_{eff} case shown in Figure 5, the lower threshold allows for a stronger sensitivity to lower WIMP masses for XENON10 relative to XENON100. The fiducial case excludes at the 90% C.L. all of the CoGeNT region and DAMA to the 5σ contour. When the 1σ uncertainties in the \mathcal{L}_{eff} measurements are taken into account, the constraints relax: DAMA is excluded to only the 3σ contour and the some of CoGeNT region at WIMP masses below 9 GeV survive. The XENON10 constraints mildly weaken if \mathcal{L}_{eff} is taken to fall linearly to zero below 3.9 keVnr, as seen in Figure 6. The fiducial case still excludes all of the CoGeNT region and DAMA to about the 4σ contour (not shown). The \mathcal{L}_{eff} 1σ band here allows the same DAMA and CoGeNT regions to survive as with the constant \mathcal{L}_{eff} case. For the case where \mathcal{L}_{eff} is zero below 3.9 keVnr, shown in Figure 7, the XENON10 constraints further weaken and approach the XENON100 constraints as the low energy events are essentially turned off and the lower XENON10 threshold becomes less relevant. Again, we note that this last case (zero \mathcal{L}_{eff} at low recoil energies) is an extremely conservative case.

As with XENON100, the potential effect of the low energy \mathcal{L}_{eff} behavior on the XENON10 constraints is limited by the imposed $\langle S1 \rangle \geq 1.0$ PE cutoff. We also show in Figure 8 the

XENON10 constraints for the three fiducial \mathcal{L}_{eff} models when this cutoff is relaxed. The same caveats apply: the nuclear recoil band cut efficiency that is used is not appropriate for the full recoil energy range that it is applied over, so these do not represent valid constraints. Again, these constraints are only used to illustrate the potential impact of the low energy \mathcal{L}_{eff} behavior on XENON10 constraints. The actual constraints when all efficiencies are accounted for properly would fall somewhere between the constraints shown in Figure 8 and those shown in Figs. (5)-(7).

With the $\langle S1 \rangle$ cutoff relaxed, Figure 8 shows how the low threshold allows for a strong XENON10 sensitivity to lower WIMP masses. This is particularly evident with the constant \mathcal{L}_{eff} case where, as can be seen in Figure 2, recoils of energy 1 keVnr yield an average $S1$ signal of 0.4 PE; $\sim 6\%$ of such recoils will produce the necessary 2+ PE. For the falling \mathcal{L}_{eff} case, that same average $S1$ signal of 0.4 PE occurs at a higher recoil energy of 2 keVnr, but this energy is still sufficiently low to provide sensitivity to low mass WIMPs. The presence of these non-trivial Poisson fluctuations at low recoil energies leads to a very strong dependence of the XENON10 constraints on the low energy \mathcal{L}_{eff} behavior. This should remain the case even when the various efficiencies are handled properly, though not quite to the degree shown in Figure 8. In particular, when the proper efficiencies are included, the XENON10 constraints in the constant and falling \mathcal{L}_{eff} cases should gain an upward curve at low WIMP masses, as seen with the other constraints, rather than the current linear appearance. These linear portions of the constraints at low WIMP masses (as they appear with the logarithmic scaling of the figure) continue to arbitrarily low WIMP masses; however, they arise from the Poisson tails of increasingly smaller energy events that would be suppressed when using the proper efficiencies.

Though we have not included it in this work, CDMS Silicon data may provide further constraints on the DAMA and CoGeNT regions and should be considered in a full discussion of compatibility between the various experimental results. The CDMS Silicon results will be considered in future work.

In summary, we have examined a number of subtleties relevant to direct detection studies of low mass WIMPs. In the interest of examining the most conservative XENON constraints, we have used the Manzur *et al.* [42] data alone in our analyses. Of the existing data sets, the Manzur *et al.* data yield the lowest values for \mathcal{L}_{eff} , implying higher recoil energy thresholds for the XENON experiments, and thereby reducing the sensitivity of XENON to low mass WIMPs. We find that, when basing the \mathcal{L}_{eff} curves on these Manzur *et al.* measurements, the behavior of \mathcal{L}_{eff} at low energies (less than 3.9 keVnr) has negligible effect on the XENON100 constraints in the regions of interest for DAMA and/or CoGeNT. For XENON100, the choice of data sets upon which the \mathcal{L}_{eff} dependence is based is more important than the extrapolated behavior of \mathcal{L}_{eff} at low recoil energies. The strongest bounds are from XENON10, rather than XENON100, due to the lower energy threshold. For reasonable choices of \mathcal{L}_{eff} and for the case of spin independent elastic scattering, we find that XENON10 is incompatible with the DAMA/LIBRA 3σ region and severely constrains the CoGeNT 7-12 GeV WIMP mass region.

Acknowledgments

C.S. is grateful for financial support from the Swedish Research Council (VR) through the Oskar Klein Centre. G.G. was supported in part by the US Department of Energy Grant DE-FG03-91ER40662, Task C. P.G. was supported in part by the NFS grant PHY-0456825

at the University of Utah. K.F. acknowledges the support of the DOE and the Michigan Center for Theoretical Physics via the University of Michigan. G.G., P.G., and C.S. thank the Galileo Galilei Institute for Theoretical Physics for the hospitality and the INFN for partial support during the completion of this work. We thank also E. Aprile, K. Arisaka, D. Hooper, and K. Zurek for helpful conversations; P. Sorensen for bringing to our attention the XENON10 $S1$ peak finding efficiency factor that was missing in the first version of this paper; L. Baudis, A. Manalaysay, G. Plante, and P. Sorensen for discussions regarding the XENON detectors and analysis; and B. Edwards and T. Sumner for discussions regarding the ZEPLIN-III \mathcal{L}_{eff} estimates.

Appendix: Comment about our choice of relevant parameters and response to critique

Shortly after the first version of our paper was released, Ref. [31] appeared commenting on it. We include here a detailed explanation of the XENON10 efficiencies and cuts we are using, as well of our use of the Manzur *et al.* measurements as a conservative choice for \mathcal{L}_{eff} (instead of the ZEPLIN-III measurements) which we believe are relevant in view of the comments expressed in Ref. [31].

1. XENON10 efficiencies and cuts

The $S1$ peak finding efficiency factor η_{S1} had not been included in the XENON10 analysis in the first version of our paper (as correctly pointed out in Ref. [31]) and has been accounted for in this revised version. However, this leads to only a moderate weakening of the XENON constraints by shifting the bound on the cross section upward by less than a factor of two. It is important to point out that including this effect does not weaken the constraints upwards in cross-section by 2-3 orders of magnitude, contrary to the claim in the critique given in Ref. [31]. One can understand the small magnitude of the effect with the following reasoning.

A valid signal event in the XENON detectors is required to produce coincident scintillation in at least two PMTs. The η_{S1} factor accounts for experimental limitations in identifying and reconstructing at least two PMT contributions to the overall $S1$ signal of a recoil event. The $S1$ signal is determined from the area under the peaks produced in the electronic readout of the PMTs. Due to digitization of the signal and intrinsic PMT performance, the size and shape of the peaks will vary⁶; see Fig. 14 of Ref. [51] for an example. Small or poorly shaped peaks may fail to be properly tagged as a PE peak in a PMT. Using the more conservative estimate found in Ref. [25], only $\eta_{S1} \approx 60\%$ of 2 PE events will have both PE peaks properly tagged and identified as coincident. As the number of PE's increases, the probability of passing the two-fold PMT requirement rapidly rises to 100%.

The significance of the η_{S1} factor on XENON10 constraints can be easily estimated. If this factor is conservatively assumed to be 60% over the entire $S1$ analysis range (2+ PE) instead of just at low $S1$, the expected number of events passing the XENON10 cuts at all energies should fall to 60% of the number of events expected without η_{S1} applied. As the

⁶ The measured $S1$ signal from a single PE as determined from the area of these peaks is 1.0 ± 0.6 PE. Thus, $S1$ can take on non-integer values even though it is given in terms of number of PE.

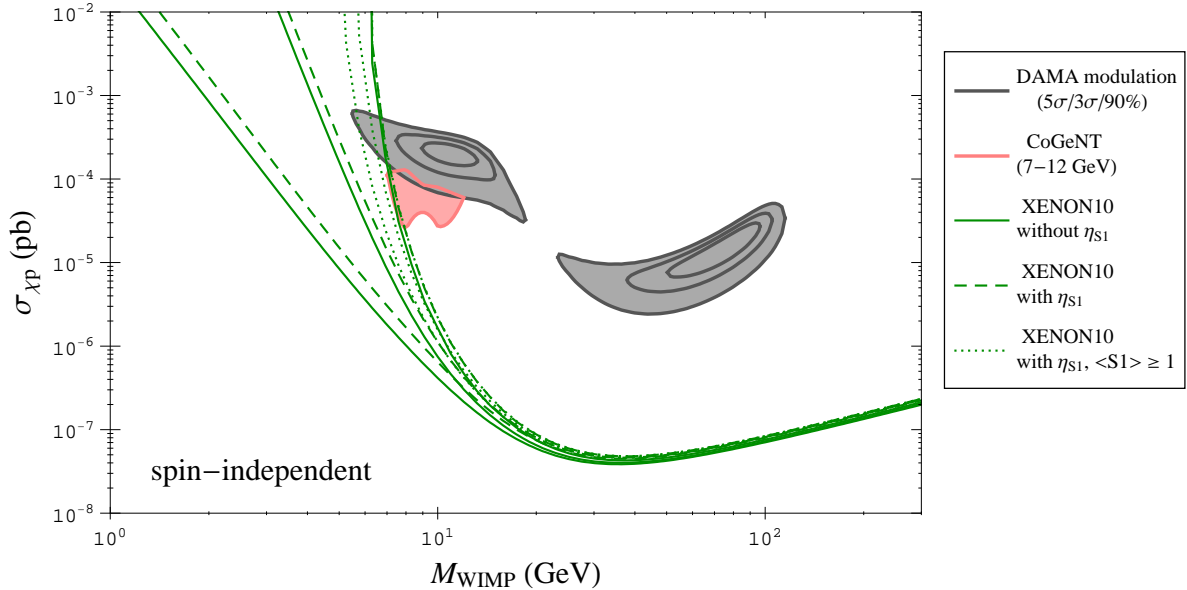


FIG. 9: Impact of (i) the $S1$ peak finding efficiency η_{S1} (dashed lines) and (ii) the $\langle S1 \rangle \geq 1$ cutoff (dotted lines) on the XENON10 constraints. Only the constraints for the fiducial (central) \mathcal{L}_{eff} models are shown; from left to right, these correspond to constant, linearly falling, and zero \mathcal{L}_{eff} below 3.9 keVnr. One can see that the second effect is by far the stronger one.

recoil rate at a particular WIMP mass is proportional to the scattering cross-section, the original recoil spectrum can be exactly reproduced by shifting the cross-section upwards by a factor of $1/0.6 \approx 1.7$. Thus, if a WIMP mass and cross-section is excluded by XENON10 at some given CL without the η_{S1} factor applied, a WIMP with the same mass and $\times 1.7$ higher cross-section would yield the same excluded spectrum with the η_{S1} factor included. In this case, the XENON10 exclusion curves shift upwards in cross-section by $\times 1.7$. As η_{S1} is higher than 60% for $S1$ larger than 2 PE, the shift in cross-section will be even smaller at heavier WIMPs where a significant number of high $S1$ events are expected.

We demonstrate in Figure 9 the weakening of the XENON10 constraints when η_{S1} is included. We show only the three fiducial (central) \mathcal{L}_{eff} models described in our paper; constraints without and with η_{S1} included are given by solid and dashed curves, respectively. For a given WIMP mass, the constraint increases by $\sim \times 1.7$ in the scattering cross-section at low WIMP masses and by less at higher WIMP masses. This is a relatively modest weakening of the constraint given the logarithmic scaling of the exclusion curve figures. Please recall that we have used the more conservative estimate of η_{S1} found in Ref. [25]. Had we used the η_{S1} factor given in Ref. [40], the change would have been even milder.

We will clarify an issue that is perhaps the source of what appears to be an erroneous application of the η_{S1} factor in Ref. [31] that yielded a greater weakening in the XENON10 results than expected. Given a recoil at some energy E_{nr} , Eqn. (1) gives the *average* expected $S1$ scintillation signal $\langle S1 \rangle$. Given the measured $S1$ in an event, Eqn. (1) can be inverted to obtain a reconstructed recoil energy E' . Due to the discreteness of the produced PE's and the variation in the $S1$ peaks, the observed prompt scintillation signal $S1$ is a random value whose expectation value is $\langle S1 \rangle$. Thus, the reconstructed recoil energy E' is also a random value and provides only an estimate of the (unknown) true recoil energy, E_{nr} .

The distinction between E' and E_{nr} is important. With the PE fluctuations and $S1$ peak variations, the true recoil energy cannot be precisely determined for any given recoil event. E' is simply an estimate of the likely recoil energy that produced an event and is understood to have some intrinsic uncertainty attached to it. At high recoil energies, $E' \approx E_{nr}$ and E' can be taken as a good approximation of the actual recoil energy. At low recoil energies, E' may differ significantly from E_{nr} on an event by event basis.

The η_{S1} factor is sometimes given as a function of recoil energy. However, as η_{S1} is really a function of the $S1$ signal, this recoil energy refers to the reconstructed energy E' of an event (recall E' and $S1$ have a 1:1 mapping through Eqn. (1)) and does *not* refer to the actual recoil energy E_{nr} . Neglecting the $S1$ peak variations and efficiencies other than η_{S1} , the fraction of events f that exceed the 2 PE threshold from scatters at a recoil energy that yields an average $S1$ signal $\langle S1 \rangle$ is given by:

$$f(\langle S1 \rangle) = \eta_{S1}(2)P(2|\langle S1 \rangle) + \eta_{S1}(3)P(3|\langle S1 \rangle) + \eta_{S1}(4)P(4|\langle S1 \rangle) \dots, \quad (\text{A.1})$$

where η_{S1} is taken as a function of $S1$ and $P(k|\langle S1 \rangle)$ is the Poisson probability of seeing k PE with an average of $\langle S1 \rangle$. If the η_{S1} factor were assumed to be a function of the actual recoil energy E_{nr} , then

$$f(\langle S1 \rangle) = \eta_{S1}(\langle S1 \rangle) [P(2|\langle S1 \rangle) + P(3|\langle S1 \rangle) + P(4|\langle S1 \rangle) \dots] \quad (\text{A.2})$$

would erroneously be taken as the fraction of events exceeding the $S1$ threshold. Use of Eqn. (A.2) in place of Eqn. (A.1) will improperly yield greatly weakened XENON10 constraints at low WIMP masses.

A second change has been made in the present version of this paper. In the first version, we assumed the same nuclear recoil band efficiency given for $2 \leq S1 \leq 5$ in Ref. [11] applied to all Poisson fluctuated events that appeared in that range. This was an optimistic assumption that may overestimate the XENON10 sensitivity at low WIMP masses. There are two data cuts relevant for low energy recoils that yield $2 \leq S1 \leq 5$: a recoil event must have $S2 \gtrsim 300$ PE ($S2$ threshold) and $1.88 \leq \log_{10}(S2/S1) \leq 2.40$ (nuclear recoil band) to be accepted as a valid event. The latter requirement is a cut designed to exclude electron recoil background events which tend to produce higher values of $S2/S1$ than nuclear recoils; the range of values here accept the lower $\sim 45\text{-}50\%$ of the distribution of $S2/S1$ expected for nuclear recoils, as determined from calibration data. At very low recoil energies, an event that produces an upward fluctuated $S1 \geq 2$ PE and would otherwise be considered a valid event might fail to produce enough $S2$ signal to pass the $S2$ threshold. The efficiency can thus be expected to fall at low recoil energies. To avoid problems with these two data cuts, we have added a cutoff to our analysis and ignore recoil energies for which $\langle S1 \rangle < 1.0$ PE. We also take the same 47% nuclear recoil band efficiency in the 2-5 PE $S1$ bin for all events in this $S1$ range stemming from low energy recoils. The addition of this cutoff significantly weakens the XENON10 constraints for WIMP masses below ~ 6 GeV for the constant and falling \mathcal{L}_{eff} models discussed in the paper, as seen by the dotted curves in Figure 9. This cutoff has a far greater impact on the constraints than the inclusion of the η_{S1} factor and is the dominant source of the change in XENON10 constraints from the first version of this paper. The third \mathcal{L}_{eff} model, zero below recoil energies of 3.9 keVnr, is unaffected by this cutoff as it does not yield any observable events at low energy anyways.

The $\langle S1 \rangle \geq 1.0$ PE cutoff and 47% assumed efficiency we have adopted here are conservative for two reasons: (1) The $S1$ and $S2$ fluctuations are independent. This means that the Poisson fluctuated events that yield higher $S1$ than the average will have lower

$S2/S1$ ratios on average and are more likely to pass the nuclear recoil band cut. The upward Poisson fluctuated events for $1.0 < \langle S1 \rangle < 2.0$ can survive this cut as much as 70-80% of the time, higher than the assumed 47%. (2) Our choice of a cutoff at $\langle S1 \rangle = 1$ PE is due to our limited ability to examine the efficiencies at lower recoil energies, not due to an expected lack of events at these low energies. We note that there will also be fluctuations in the number of ionization electrons that lead to the $S2$ signal⁷; even at very low recoil energies, there may be a non-zero probability of both $S1$ and $S2$ exceeding their respective thresholds and producing events in the analysis region that pass all cuts. For the constant \mathcal{L}_{eff} case at a WIMP mass of 5 GeV and scattering cross-section of 10^{-2} pb, a point not excluded by the conservative bounds in Figure 9, about 20,000 recoils would be expected for recoil energies corresponding to $0.5 \leq \langle S1 \rangle \leq 1.0$. Even with a very small efficiency for such recoils, some number of these events would be expected to have fluctuations that put them in the XENON10 analysis region. If the nuclear recoil band efficiency were only $\sim 1\%$ over this range, 10+ events would be expected to pass the various cuts; the lack of such events in the data would rule out these WIMP parameters.

2. ZEPLIN-III \mathcal{L}_{eff} models

Refs. [32] and [31] suggest using the the ZEPLIN-III \mathcal{L}_{eff} measurement [43], represented as a band in Fig. 1 of Ref. [32], as a conservative choice of \mathcal{L}_{eff} . Thus, we discuss here this possibility.

ZEPLIN fits a nonlinear \mathcal{L}_{eff} model to their broad spectrum nuclear recoil calibration data to obtain \mathcal{L}_{eff} curves that were used in their analysis. These fits suggest a constant \mathcal{L}_{eff} at recoil energies above ~ 30 keVnr, with \mathcal{L}_{eff} sharply falling at energies below ~ 20 keVnr and approaching zero at $\sim 7-8$ keVnr; see Figure 15 of Ref. [43] and the accompanying text. The suggestion has been made [31] that \mathcal{L}_{eff} should be taken to be zero below ~ 8 keVnr as a conservative model of \mathcal{L}_{eff} . This \mathcal{L}_{eff} model would yield significantly weaker XENON constraints relative to what we have referred to as conservative models based on the Manzur *et al.* measurements of \mathcal{L}_{eff} [42].

We have several reservations about using this ZEPLIN inspired \mathcal{L}_{eff} model. First, ZEPLIN does not provide estimates of \mathcal{L}_{eff} below ~ 7 keVnr and, in fact, states they are limited in constraining \mathcal{L}_{eff} at these low energies (in the caption of their Fig 15, it is said that “The constraints become very weak outside the energy ranges shown.”). Second, neither the technical details of ZEPLIN’s curve-fitting nor estimates of the statistical and systematic uncertainties are provided in their paper. Without these, it is unclear with which degree of certainty the low energy ($\sim 7-10$ keVnr) end of the ZEPLIN-III curves should be treated. Several sources of error may contribute to the level of uncertainty in these \mathcal{L}_{eff} estimates. One is the errors associated with the Monte Carlo used to compare with data, which are difficult to quantify since they can arise from inaccuracies in the inelastic neutron scattering data used in the Géant4 code and obtained from an international library of such data. Another issue are systematic errors associated with uncertainties in the position of the neutron source near the detector during calibration runs. If the uncertainties are large, then ZEPLIN does not have the statistical power to determine the \mathcal{L}_{eff} behavior at low recoil energies and one should base the \mathcal{L}_{eff} curves on measurements that have a better statistical power to

⁷ The $S2$ threshold of ~ 300 PE corresponds to about 12 ionization electrons, each of which produce ~ 25 PE.

analyze this \mathcal{L}_{eff} behavior, such as the Manzur *et al.* data. If the uncertainties are small so that the ZEPLIN curve is expected to be an accurate representation of the \mathcal{L}_{eff} behavior at low energies, then there is a very serious discrepancy between the ZEPLIN and Manzur *et al.* results (see below). The ZEPLIN collaboration claims no leverage on \mathcal{L}_{eff} below about 8 keVnr and do not suggest that it goes to zero in that energy range⁸ [44]. The recoil energy interval in the ZEPLIN analysis of 10.7–30.2 keVnr does not include the low energy, low \mathcal{L}_{eff} end of their \mathcal{L}_{eff} curves. In this analysis region, the ZEPLIN \mathcal{L}_{eff} curves are compatible with the Manzur *et al.* measurements within the 1-2 σ level.

Furthermore, the ZEPLIN inspired model proposed by Ref. [31], taking $\mathcal{L}_{\text{eff}} = 0$ below recoil energies of ~ 8 keVnr, is strongly incompatible with the Manzur *et al.* measurements as well as other fixed energy neutron scattering measurements such as those of Aprile *et al.* [41]. We reiterate that our choice to use the Manzur *et al.* data in our analysis was due to the lower \mathcal{L}_{eff} values that give more conservative XENON constraints and should not be construed as an indication that we regard this data as the most accurate available. We make no contribution to the discussion regarding the accuracy of the various low energy recoil measurements from neutron beam scattering. See Ref. [52] for a discussion of the various potential issues which may affect the \mathcal{L}_{eff} determinations in these experiments. In any case, much of the discussion below regarding the incompatibility of the Manzur *et al.* data with $\mathcal{L}_{\text{eff}} = 0$ applies also to the Aprile *et al.* measurements.

Given the Manzur *et al.* measurement of *e.g.* $\mathcal{L}_{\text{eff}} = 0.073_{-0.025}^{+0.034+0.018}$ (statistical and systematic errors, respectively) at a recoil energy of 3.9 ± 0.9 keVnr, one might naively conclude this measurement is consistent with $\mathcal{L}_{\text{eff}} = 0$ at the ~ 2 -3 σ level. However, the \mathcal{L}_{eff} value and errors are determined from a χ^2 fit to the data as a function of \mathcal{L}_{eff} . The χ^2 versus \mathcal{L}_{eff} curves, such as shown in Fig. 11(c) of Ref. [42] for a recoil energy of 6 keVnr, are not symmetric about the minima (which provide the central values), but rise very rapidly as \mathcal{L}_{eff} becomes small, effectively diverging at $\mathcal{L}_{\text{eff}} = 0$. The result is that the Manzur *et al.* measurements (four of which are below recoil energies of 7 keVnr) are incompatible with $\mathcal{L}_{\text{eff}} = 0$ recoil energies of ~ 8 keVnr, as this would yield χ^2 values that are incompatible at far higher than the 3 σ level. We consider the Manzur *et al.* measurements more reliable than the ZEPLIN-III estimate of \mathcal{L}_{eff} at low energies.

To illustrate the incompatibility of the Manzur *et al.* data with $\mathcal{L}_{\text{eff}} = 0$, one can understand the χ^2 behavior as follows. Manzur *et al.* measured \mathcal{L}_{eff} at several recoil energies by observing the scintillation response in a Xenon detector for neutrons from a beam of fixed energy (2.8 MeV) that scatter in a fixed direction; the recoil energy is fixed by the angle of scatter⁹. If \mathcal{L}_{eff} is non-zero at the recoil energy corresponding to a particular scattering angle, a histogram of the $S1$ from observed events will generate a peak due to scintillation from the single scatter events in the detector. The primary background is double scatter-

⁸ ZEPLIN used a 9-point spline function to model the curves and a classical maximum likelihood method using a grid scan across a 9 point parameter space to make sure they found a global minimum [44]. ZEPLIN only fit their data down to 2 keVee, thus could infer nothing below about 6 keVnr. The middle curve in their Fig. 15 [43] gives the “best fit” and the outer two curves indicate regions where “similar goodness-of-fit values” were obtained as stated in the caption; the band does not represent a region with a particular statistical significance (*e.g.* 1- σ or 90% C.L.) in the uncertainties.

⁹ Due to the geometry of the Xenon detector and width of the scintillator used to detect the scattered neutrons, each measurement is sensitive to a finite range of recoil angles and, thus, recoil energies. The uncertainties in the recoil energies given for each \mathcal{L}_{eff} measurement arise mainly from this range.

ing neutrons which can reach the neutron scintillator located at the fixed angle from the neutron beam, but scatter with a different energy than expected for single scatter neutrons that reach the neutron scintillator; one of the two scatters must occur outside of the active volume for the event to be mistaken as a single scatter. These double scattering neutron events are expected to occur at an almost negligible rate compared to the single scatter signal events. In addition, these double scatter events produce a fairly flat $S1$ distribution, not a peak (see *e.g.* Figure 9 of Ref. [42]). Figures 11(a) and 11(c) of Ref. [42] show an $S1$ histogram and corresponding χ^2 versus \mathcal{L}_{eff} curve, respectively, for recoils centered at 6 keVnr. The histogram shows a peak of ~ 700 events (consistent with scintillation from single scatter signal events) with a negligible flat contribution (expected from any significant double scatter background). The χ^2 in this case is minimized at $\mathcal{L}_{\text{eff}} \approx 0.06$. At lower \mathcal{L}_{eff} , the χ^2 grows rapidly for this reason: it is difficult to account for this ~ 700 scintillation event peak if the nuclear recoils produce little to no scintillation. Note the systematic issues discussed in Manzur *et al.* generally affect the interpretation of which \mathcal{L}_{eff} would produce such a peak, but do not provide significant alternate mechanisms for producing such a peak aside from the scintillation from low energy recoils (scintillation that can only be produced if $\mathcal{L}_{\text{eff}} \not\approx 0$). Thus, while determining the value of \mathcal{L}_{eff} based on the size and shape of such $S1$ peaks may be limited by statistics or biased by systematic effects, the simple presence of such a peak is strong evidence that \mathcal{L}_{eff} is non-zero.

Given that Manzur *et al.* have observed scintillation peaks at multiple recoil energies over $\sim 4\text{-}8$ keVnr, we consider the “conservative” \mathcal{L}_{eff} model suggested in Refs. [32] and [31], with $\mathcal{L}_{\text{eff}} = 0$ below ~ 8 keVnr, to be grossly incompatible with existing data and therefore unrealistically conservative.

-
- [1] R. Bernabei *et al.*, Eur. Phys. J. C **67**, 39 (2010) [arXiv:1002.1028 [astro-ph.GA]].
 - [2] A. K. Drukier, K. Freese, D. N. Spergel, Phys. Rev. **D33**, 3495-3508 (1986).
 - [3] K. Freese, J. A. Frieman, A. Gould, Phys. Rev. **D37**, 3388 (1988).
 - [4] G. Gelmini and P. Gondolo, arXiv:hep-ph/0405278.
 - [5] P. Gondolo and G. Gelmini, Phys. Rev. D **71**, 123520 (2005) [arXiv:hep-ph/0504010].
 - [6] R. Bernabei *et al.* [DAMA Collaboration], Eur. Phys. J. C **56**, 333 (2008) [arXiv:0804.2741 [astro-ph]].
 - [7] C. Savage, G. Gelmini, P. Gondolo and K. Freese, JCAP **0904**, 010 (2009) [arXiv:0808.3607 [astro-ph]].
 - [8] Z. Ahmed *et al.* [CDMS Collaboration], Phys. Rev. Lett. **102**, 011301 (2009) [arXiv:0802.3530 [astro-ph]].
 - [9] J. Angle *et al.* [XENON Collaboration], Phys. Rev. Lett. **100**, 021303 (2008) [arXiv:0706.0039 [astro-ph]].
 - [10] C. E. Aalseth *et al.* [CoGeNT collaboration], arXiv:1002.4703 [astro-ph.CO].
 - [11] J. Angle *et al.* [XENON10 Collaboration], Phys. Rev. D **80**, 115005 (2009) [arXiv:0910.3698 [astro-ph.CO]].
 - [12] E. Aprile *et al.* [XENON100 Collaboration], arXiv:1005.0380 [astro-ph.CO].
 - [13] N. Bozorgnia, G. B. Gelmini and P. Gondolo, arXiv:1006.3110 [astro-ph.CO].
 - [14] Z. Ahmed *et al.* [The CDMS-II Collaboration], arXiv:0912.3592 [astro-ph.CO]; Z. Ahmed *et al.* [The CDMS-II Collaboration], Science **327**, 1619 (2010).

- [15] A. Bottino, F. Donato, N. Fornengo and S. Scopel, Phys. Rev. D **81**, 107302 (2010) [arXiv:0912.4025 [hep-ph]].
- [16] J. Kopp, T. Schwetz and J. Zupan, JCAP **1002**, 014 (2010) [arXiv:0912.4264 [hep-ph]].
- [17] A. L. Fitzpatrick, D. Hooper and K. M. Zurek, arXiv:1003.0014 [hep-ph].
- [18] S. Chang, J. Liu, A. Pierce, N. Weiner and I. Yavin, arXiv:1004.0697 [hep-ph].
- [19] F. Petriello and K. M. Zurek, JHEP **0809**, 047 (2008) [arXiv:0806.3989 [hep-ph]].
- [20] A. Bottino, F. Donato, N. Fornengo and S. Scopel, Phys. Rev. D **78**, 083520 (2008) [arXiv:0806.4099 [hep-ph]].
- [21] S. Chang, A. Pierce and N. Weiner, Phys. Rev. D **79**, 115011 (2009) [arXiv:0808.0196 [hep-ph]].
- [22] D. Hooper, F. Petriello, K. M. Zurek and M. Kamionkowski, Phys. Rev. D **79**, 015010 (2009) [arXiv:0808.2464 [hep-ph]].
- [23] S. Andreas, C. Arina, T. Hambye, F. S. Ling and M. H. G. Tytgat, arXiv:1003.2595 [hep-ph]; note the XENON100 discussion first appears in arXiv version 3.
- [24] S. Yellin, Phys. Rev. D **66**, 032005 (2002) [arXiv:physics/0203002].
- [25] P. Sorensen, presented at the 2010 Light Dark Matter Workshop, UC Davis, <http://particle.physics.ucdavis.edu/seminars/data/media/2010/apr/sorensen.pdf>; see the blue curve on page 6.
- [26] P. Sorensen, arXiv:1007.3549 [astro-ph.IM].
- [27] J. I. Collar, private correspondence.
- [28] M. C. Smith *et al.*, Mon. Not. Roy. Astron. Soc. **379**, 755 (2007) [arXiv:astro-ph/0611671].
- [29] M. J. Reid *et al.*, Astrophys. J. **700**, 137 (2009) [arXiv:0902.3913 [astro-ph.GA]].
- [30] C. Savage, K. Freese, P. Gondolo and D. Spolyar, JCAP **0909**, 036 (2009) [arXiv:0901.2713 [astro-ph]].
- [31] J. I. Collar, arXiv:1006.2031 [astro-ph.CO].
- [32] J. I. Collar and D. N. McKinsey, arXiv:1005.0838 [astro-ph.CO].
- [33] The XENON Collaboration, arXiv:1005.2615 [astro-ph.CO].
- [34] J. I. Collar and D. N. McKinsey, arXiv:1005.3723 [astro-ph.CO].
- [35] F. Arneodo *et al.*, Nucl. Instrum. Meth. A **449**, 147 (2000).
- [36] R. Bernabei *et al.*, Eur. Phys. J. direct C **3**, 11 (2001).
- [37] D. Akimov *et al.*, Phys. Lett. B **524**, 245 (2002) [arXiv:hep-ex/0106042].
- [38] E. Aprile *et al.*, Phys. Rev. D **72**, 072006 (2005) [arXiv:astro-ph/0503621].
- [39] V. Chepel *et al.*, Astropart. Phys. **26**, 58 (2006).
- [40] P. Sorensen *et al.*, Nucl. Instrum. Meth. A **601**, 339 (2009) [arXiv:0807.0459 [astro-ph]].
- [41] E. Aprile *et al.*, Phys. Rev. C **79**, 045807 (2009) [arXiv:0810.0274 [astro-ph]].
- [42] A. Manzur, A. Curioni, L. Kastens, D. N. McKinsey, K. Ni and T. Wongjirad, Phys. Rev. C **81**, 025808 (2010) [arXiv:0909.1063 [physics.ins-det]].
- [43] V. N. Lebedenko *et al.*, Phys. Rev. D **80**, 052010 (2009) [arXiv:0812.1150 [astro-ph]].
- [44] T. Sumner for the ZEPLIN Collaboration, private correspondence.
- [45] H. Sekiya, M. Minowa, Y. Shimizu, Y. Inoue and W. Sukanuma, Phys. Lett. B **571**, 132 (2003) [arXiv:astro-ph/0307384]; H. Sekiya, M. Minowa, Y. Shimizu, W. Sukanuma and Y. Inoue, arXiv:astro-ph/0405598; H. Sekiya, M. Mionwa, Y. Shimizu, W. Sukanuma and Y. Inoue, arXiv:astro-ph/0411215.
- [46] E. M. Drobyshevski, Mod. Phys. Lett. A **23** (2008) 3077 [arXiv:0706.3095 [physics.ins-det]].
- [47] R. Bernabei *et al.*, Eur. Phys. J. C **53**, 205 (2008) [arXiv:0710.0288 [astro-ph]].
- [48] J. Lindhard, Kongel. Dan. Vidensk. Selsk., Mat.-Fys. Medd. **34** No. 14 (1965).

- [49] D. S. Gemmell, *Rev. Mod. Phys.* **46**, 129 (1974).
- [50] G. Hobler, *Radiation effects and defects in solids* **139**, 21 (1996); G. Hobler, *Nucl. Instrum. Meth. B* **115**, 323 (1996).
- [51] E. Aprile *et al.* [XENON Collaboration], arXiv:1001.2834 [astro-ph.IM].
- [52] A. Manalaysay, arXiv:1007.3746 [astro-ph.IM].